RSC Advances

PAPER

View Article Online
View Journal | View Issue

Cite this: *RSC Adv.*, 2026, **16**, 27242

Photoinactivation of *S. aureus* biofilms using porphyrin conjugates with green-synthesized TiO_2 immobilized on waste polystyrene

Nonkululeko Malomane,[a] Nkgameleng K. Mokhonoana,[a] Christian I. Nkanga,[b] Ojodomo J. Achadu,[c] Richard M. Moutloali[a] and Muthumuni Managa *[a]

Received 4th January 2026
Accepted 22nd April 2026

DOI: 10.1039/d6ra00069j

rsc.li/rsc-advances

Waterborne infections remain a global concern, exacerbated by biofilms in water storage systems that resist chlorine disinfection. In this study, antimicrobial photodynamic inactivation was investigated using novel porphyrin-TiO_2 nanoconjugates prepared from green-derived TiO_2 nanoparticles using *Citrus sinensis* extracts and immobilized on waste polystyrene (PS) for the first time. Metal-free 5,10,15-*tris*(4-bromophenyl)-20-(4-carboxyphenyl)porphyrin (**1**) and its ClIn(III) derivative (**2**) were conjugated to TiO_2, then immobilized on PS. Characterization by FTIR, EDX, TGA, SEM, TEM, and UV-vis confirmed successful formation of thermally stable and spherical nanostructures. Moreover, photophysical studies showed that metalation reduced fluorescence quantum yield (Φ_F) from 0.01 (**1**) to <0.01 (**2**) due to heavy atom effect) while boosting singlet oxygen yield ((Φ_Δ) from 0.68 (**1**) to 0.85 (**2**)–0.90 (**2**-TP). Free 2-TP achieved 0.0006% *S. aureus* survival percentage while PS-immobilized versions reached 2.5% under 30 minutes visible light exposure. These sustainable, high-efficiency materials advance biofilm-resistant water treatment for resource-limited settings.

1 Introduction

Waterborne infections continue to threaten human health globally, contributing to 1.4 million unsafe Water, Sanitation, and Hygiene (WASH)-related annual deaths worldwide.[1] In Sub-Saharan Africa, this equates to 115 deaths per hour from poor sanitation and contaminated water.[2] Contributing factors include bacteria such as *S. aureus*, prevalent in stored household water and driving antimicrobial resistance.[3] A critical, yet understudied factor that perpetrates the spread of waterborne infections, is the biofilm formation on the surfaces of water storage systems.[4] Households from resource-constrained areas, such as rural settlements, are at risk of waterborne diseases.[5] They collect and store water that may already be contaminated with pathogenic bacteria or can be contaminated during collection, transportation, storage and use. Suspended bacteria attach to the surface inside and to each other during storage using self-made extracellular substances (EPS).[6] The bacteria then multiply and detach in a continuous process. Besides offering protection to bacteria, biofilms play a significant role in lowering the efficiency of disinfectants such as chlorine.[6,7] They also perpetrate the development and spread of resistance within the bacterial community.[8] This greatly deteriorates water quality and necessitates the development of new water disinfection methods.

Antimicrobial photodynamic inactivation (aPDI) has shown great potential for inactivation of bacteria in water.[9] In this technique, microorganisms are inactivated by shining light on a photosensitizer that generates reactive oxygen species, causing oxidative stress to the microbe.[10] Research on the optimization of photosensitizers to improve their properties is topical. An ideal photosensitizer should produce reactive oxygen species efficiently to cause microbial cell death within a short space of time.[6,11] Porphyrins with bromine halogen substituents and diamagnetic heavy metals such as indium have been found to improve aPDI efficiency due to heavy atom effect.[12] Furthermore, several studies have shown that adsorption of porphyrins onto UV light active TiO_2 nanoparticles improves their overall performance as photosensitizers.[13,14] This is achieved by the ability of porphyrins to enhance the absorbance of the overall system in the visible range, as well as improve charge separation of TiO_2, thus improving the antimicrobial activity.[15] In addition to these photocatalytic enhancements, green synthesized TiO_2 nanoparticles alone have been reported to have intrinsic antimicrobial properties, with greater performance than conventionally synthesized TiO_2

[a]*Institute for Nanotechnology and Water Sustainability (iNanoWS), Florida Campus, College of Science, Engineering and Technology, University of South Africa, Johannesburg 1710, South Africa. E-mail: managme@unisa.ac.za*

[b]*Centre de Recherche en Nanotechnologies Appliquées aux Produits Naturels (CReNAPN), Department of Medicinal Chemistry and Pharmacognosy, Faculty of Pharmaceutical Sciences, University of Kinshasa, B.P. 212, Kinshasa XI, Democratic Republic of the Congo*

[c]*School of Health and Life Sciences & , National Horizon Centre, Teesside University, Tees Valley, Middlesbrough TS1 3BX, UK*

nanoparticles without any light against *S. aureus*, *E. coli* and *P. aeruginosa*.[16]

Many light-driven studies utilized TiO_2-porphyrin in suspension.[17–19] However, this poses risk of photosensitizer leaching and secondary contamination of water and may require additional steps of separation and recovery of the nanoparticles after disinfection.[6] To foster real-life applications in the disinfection of water storage systems, studies have used supports such as quartz wool, polyvinylpyrrolidone, polyactic acid, bentonite and chitosan.[13,20–22] In addition to this, another study reported that polystyrene (PS) polymer provides stable support to other porphyrin conjugates in electrospun nanofibers.[23]

In this study, the photophysical and photodynamic antimicrobial properties of previously reported 5,10,15-*tris*-(4-bromopheyl)-20-(4-carboxyphenyl)porphyrin (**1**) (Scheme 1) and its indium chloride derivative (**2**) adsorbed onto green synthesized TiO_2 nanoparticles using orange fruit (*Citrus sinensis*) peel extract (T1) and juice (TP) were explored against environmental *S. aureus* biofilms.[15,24] These porphyrin-TiO_2 conjugates represent novel combinations, which were physically immobilized, for the first time, onto waste PS from used PS cups. Waste PS was chosen in contribution to climate change mitigation strategies as it poses a significant environmental health issue due to its non-biodegradable characteristic. The non-biodegradable property of PS serves as an advantage in this study so that the immobilized photosensitizers do not get degraded by the microbes during inactivation.

2 Experimental

2.1 Conjugation of TiO_2 nanoparticles with 1 and 2

Compounds **1**, **2**, TJ and TP were synthesized, purified and characterized as recently reported.[15,24] Metal-free and In(III) porphyrins were conjugated non-covalently with TiO_2 nanoparticles following reported procedures.[25] **1** or **2** (0.025 g) was dissolved in DMF (10 mL), followed by addition of 100 mg TP or TJ. The mixture was stirred for 24 hours at 50 °C to facilitate adsorption of the porphyrin molecules onto the surface of TiO_2 nanoparticles. The conjugates were washed several times with ethanol until the washing solution became clear. The conjugates collected *via* centrifugation were then air-dried overnight at room temperature. The conjugates were labelled **1**-TP, **1**-TJ for the metal free porphyrin conjugates with TiO_2 nanoparticles synthesized from orange peel extract and orange juice, respectively, and **2**-TP, **2**-TJ for the In(III) porphyrin conjugates.

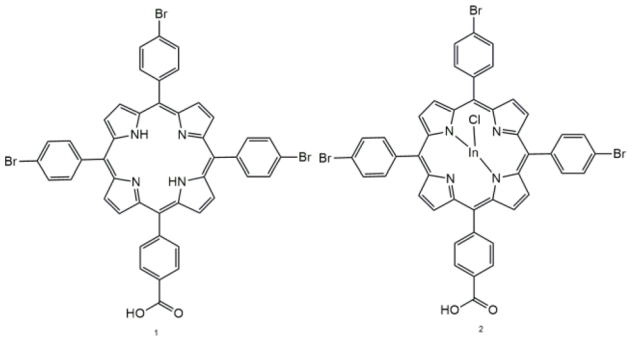

Scheme 1 Chemical structures as-synthesized porphyrins labelled 5,10,15-tris-(4-bromopheyl)-20-(4-carboxyphenyl) porphyrin (**1**) and ClIn(III) 5,10,15-*tris*-(4-bromopheyl)-20-(4-carboxyphenyl)porphyrin (**2**).

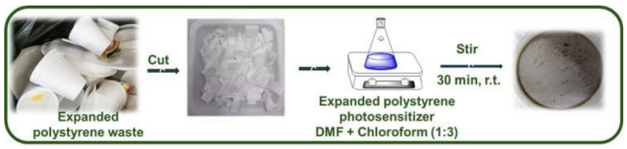

Scheme 2 Immobilization of the photosensitizers (**1**, **2**, TP, TJ, **1**-TP, **1**-TJ, **2**-TP, or **2**-TJ) onto PS waste.

2.2 Immobilization onto PS waste

2.5 g PS was dissolved into a mixture of chloroform and DMF (1 : 3), followed by the addition of the photosensitizer (**1**, **2**, TP, TJ, **1**-TP, **1**-TJ, **2**-TP, or **2**-TJ) (0.025 mg) and stirring for 30 minutes until a homogeneous mixture was obtained (Scheme 2). This was then poured into glass Petri dishes, and the solvents were allowed to evaporate in air.

2.3 Photoinactivation studies

2.3.1 Sampling and bacterial isolation. Water samples were collected from a pond at the University of South Africa, Florida campus located in Gauteng, South Africa, using sterile 250 mL glass water sampling bottles. The open pond is stagnant and mimics household water storage conditions, vulnerable to contamination by airborne microbes, bird faeces as well as physical human activities. Prior to sampling, the bottles were thoroughly washed with soap and water and then sterilized by autoclaving for 15 min at 120 °C. On-site physical parameters (pH, conductivity, TDS, turbidity) were measured and *S. aureus* bacteria were isolated from the water immediately using mannitol salt agar plates by incubating for 48 h at 37 °C. Sequential streaking ensured formation of pure yellow colonies (mannitol fermentation) in mannitol salt agar. The full bacterial characterization (morphology, Gram stain, catalase, 16 s rRNA sanger sequencing for characterization of the bacteria are detailed in the SI.

Prior to inactivation, 30% glycerol stock solution of *S. aureus* previously isolated (SI) and stored at −20 °C freezer was placed at room temperature to thaw. A full loop of *S. aureus* stock was aseptically streaked onto mannitol salt agar plate and incubated at 37 °C for 24 hours to obtain fresh bacterial culture. Subsequently, a fresh bacterial stock solution was prepared by inoculating in nutrient broth (6 mL) and incubating (24 h, 37 °C, 200 rpm shaking). When the optical density (OD) of the bacteria at 600 nm reached 0.8, the bacteria were then centrifuged at 4000 rpm for 5 minutes and washed twice with Phosphate-buffered saline (PBS) to remove the broth. The supernatant was decanted, and pellet was stored in 100 mL PBS at a 10^{-2} dilution factor at −2 °C. The working concentration of the bacteria was optimized by serial dilution plating (10^{-7} dilution

factor in PBS), until less than 300 colonies were obtained in mannitol salt agar.

2.3.2 aPDI studies against freely suspended bacteria using free materials. The aPDI studies were conducted using the reported procedures with modifications.[23,26] The colony counting method gave inconsistent unreliable results, therefore, the optical density method (turbimetric analysis) was used to determine the efficiency of the photosensitizers. Photosensitizer concentration optimization was done by exposing the bacteria to 0.05, 0.10, 0.25, 0.5 and 1.0 mg mL^{-1} of the photosensitizer and 0.25 mg mL^{-1} was chosen as optimal concentration. Photosensitizer stocks (0.25 mg mL^{-1}); **1**, **2**, TP, TJ, **1**-TP, **1**-TJ, **2**-TP, and **2**-TJ were then prepared in PBS. 150 μL aliquots of the bacterial suspension in PBS were added into sterile 12-well microplates, followed by 100 μL aliquots of each photosensitizer. The initial absorbance of the bacteria was taken using a spectrophotometer. For each experiment, two sets of 12-well plates with similar contents were prepared for dark and light experiments, respectively, and the experiments were performed in triplicates.

Both plates were subjected to a 60-minutes aerobic pre-incubation period in the dark at 37 °C to allow localization of the photosensitizers.[27] One plate was subjected to irradiation for 30 minutes, while the other was left in the dark for the same period, with 5 minutes sampling intervals. 100 μL bacteria-photosensitizer suspension was taken out and added to 96-plates, followed by addition of 150 μL nutrient broth and incubation (24 h, 37 °C) in a rotary shaker. The final concentration of the bacteria was determined by checking the absorbance. The controls without photosensitizers were used to correct the viable bacteria. An LED-mounted irradiation chamber equipped with M415L4 LED with a continuous irradiance yielding a maximum of 15.6 μW mm^{-2} was used. The survival percentage was calculated using the formula:

$$\text{Survival percentage} = \frac{A_T - A_B}{A_C - A_B} \times 100 \quad (1)$$

where A_T is the absorbance of the bacteria after inactivation, A_B is the absorbance of the photosensitizer control without any bacteria, and A_C is the absorbance of the control bacteria without any photosensitizer.

2.3.3 aPDI studies against biofilm bacteria using free materials. The antibacterial activities of **1**, **2**, TP, TJ, **1**-TP, **1**-TJ, **2**-TP, and **2**-TJ as well as bare-PS were investigated using single-species bacterial biofilms of *S. aureus* following the reported protocol.[28] The bacterial inoculate was prepared using Tryptic soy broth, and 100 μL suspension was placed in 96-well plates and allowing a 5-days incubation period at 37 °C. To encourage biofilm growth, unbound cells were rinsed with PBS, and the wells were replenished with new Tryptic soy after 18 h. The biofilm-coated wells were subjected to three PBS washes and a 30-minutes air drying period.

For illumination, 1.0 mg mL^{-1} of each photosensitizer, optimized as described above, was placed into biofilm-coated wells and incubated for 1 hour at 37 °C in a rotary shaker.[29] The wells were then illuminated for 30 minutes at 5 minutes sampling intervals times. Following this, the cells were stained with 1% aqueous crystal violet (CV) solution, and excess CV removed by three PBS washes after 30 min, and fresh Tryptic soy broth added into the wells to determine the survival fraction of biofilms by checking their absorbance and comparing them to those without photosensitizers.[30] On the other hand, PBS was added to dilute the samples maintained in the dark and then each solution was carefully inoculated on Tryptic soy broth, followed by 18 h incubation at 37 °C. The controls without photosensitizers were used to correct the viable bacteria and the optical densities of the viable bacteria were calculated at 600 nm. Each of these experiments were done in triplicates.

2.3.4 Photoinactivation of freely suspended bacteria using immobilized photosensitizers. The photodynamic antimicrobial activity of the photosensitizers immobilized onto waste PS, **1**-PS, **2**-PS, TP-PS, TJ-PS, **1**-TP-PS, **1**-TJ-PS, **2**-TP-PS, and **2**-TJ-PS, were examined against environmental *S. aureus* in suspension according to a modified procedure adopted from literature.[31] PS alone was used as negative control. In a typical experiment, one 1 × 1 cm^2 piece of each of the immobilized photosensitizers was separately placed in sterile 12-well microplates. 150 μL PBS suspension of was added into the wells containing the photosensitizers onto PS. After incubation of 60 min, the wells were exposed to a light illumination for 30 min, while the other pairs of wells were left in the dark for the same duration. For each experiment, two sets of 12-well plates with similar contents were prepared for dark and light experiments, respectively, and the experiments were performed in triplicates. Afterwards, the immobilized photosensitizers from all wells were taken out of the bacterial solution and were placed into 5 mL of sterilized PBS solution. The solution was shaken vigorously for 1 min. 100 μL bacteria was taken into 96 well plates, followed by addition of 150 μL nutrient broth and incubated for 24 h in a rotary shaker at 37 °C. The final concentration of the bacteria was determined by checking the absorbance. The bacterial solutions without immobilized photosensitizers were used as negative controls to correct the viable bacteria and the optical densities of the viable bacteria were calculated at 600 nm. The survival percentage was calculated using the eqn (1).

2.3.5 Photoinactivation of biofilm bacteria using immobilized photosensitizers. The photodynamic antimicrobial activity of the photosensitizers immobilized onto waste PS, **1**-PS, **2**-PS, TP-PS, TJ-PS, **1**-TP-PS, **1**-TJ-PS, **2**-TP-PS, and **2**-TJ-PS, were examined against single species *S. aureus* biofilms. The biofilms were prepared and illuminated as described above. In a typical experiment, one 1 × 1 cm^2 piece of each of the immobilized photosensitizer was separately placed in biofilm coated wells. For each experiment, two sets of 96-well plates with similar contents were prepared for dark and light experiments, respectively, and the experiments were performed in triplicates. After incubation of 60 min, the wells were exposed to a light illumination for 30 min with 5 minutes sampling intervals while the other pairs of wells were left in the dark for the same duration. Afterwards, the immobilized photosensitizers were removed from all wells. Following this, the cells were stained with 1% aqueous CV solution, and excess CV removed by three PBS washes after 30 min, and fresh PBS added into the wells to determine the survival fraction of biofilms by checking their

absorbance and comparing them to those without photosensitizers.[30] On the other hand, PBS was added to dilute the samples maintained in the dark and then each solution was carefully inoculated on agar plates, followed by 18 h incubation at 37 °C. The controls without photosensitizers were used to correct the viable bacteria and the optical densities of the viable bacteria were calculated at 600 nm. Each of these experiments were done in triplicates.

3 Results and discussion

3.1 Fourier transform infrared spectroscopy (FTIR)

The functional groups within the materials were studied using FTIR. Fig. 1 shows the FTIR spectra of PS, TJ, **2**-TJ, **2**-TJ-PS as well as that of previously reported **2** (ref. 24) as examples. The results for TJ showed a strong peak below 1000 cm^{-1}, indicating the presence of Ti–O bonds in the anatase phase of TiO_2.[32] Broad absorption bands at 3400 and 1635 cm^{-1} revealed hydroxyl groups (O–H or Ti–OH) due to water moisture adsorbed on the TiO_2 surface.[33] Notably, nanoparticles TP and TJ exhibited an additional peak at 1392 cm^{-1} (C–C/C=C), attributed to organic residues from calcination, consistent with previous findings.[16] The FTIR spectra of **2** shows characteristic peaks for the carboxylic acid group (1691 cm^{-1}) and pyrrole ring (1510, 1424, 1280, and 1010 cm^{-1}). After conjugation, similar changes were observed for all conjugates, with decreased intensity and shifted C=O and C–O bands. Two new intense bands emerged at 1650 and 1394 cm^{-1}, indicating the formation of carboxylate species ($\nu(-CO_2^-)$), due to chemisorption onto the TiO_2 surface. This interaction may contribute to the enhanced activity of the conjugated systems, consistent with previous reports.[34]

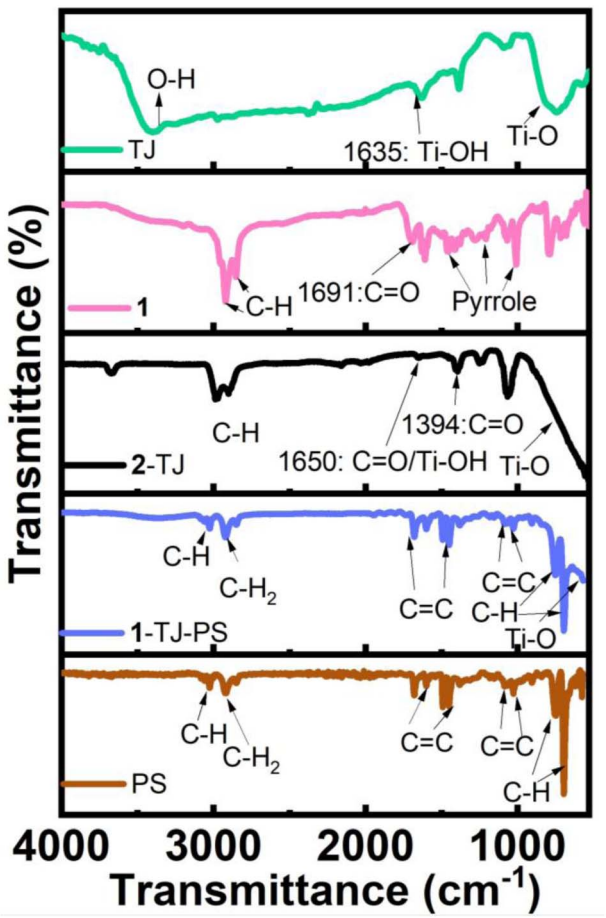

Fig. 1 FTIR spectra of PS, **2**, TJ, **2**-TJ, **2**-TJ-PS as an example.

For PS, the C=C peaks appear at 1600, 1492, and 1451 cm^{-1}, indicating the presence of expected benzene rings in PS.[35] The transmission band at 3025 cm^{-1} corresponds to the stretching vibrational modes of aromatic C–H groups, and the peak at 2941 cm^{-1} corresponds to vibrational modes of $C–H_2$ due to methylene groups.[35,36] Typical out-of-plane bending vibration C–H peaks occur at 754 and 694 cm^{-1}, confirming only one substituent in the benzene ring.[36] These peaks are not present in **2**-TJ and TJ alone and appear to overlap with Ti–O peaks in **2**-TJ-PS, confirming the presence of the conjugates on the PS. A previous study by Naik *et al.*[37] found that immobilizing of iron and cobalt metalloporphyrins onto PS physically does not significantly alter its FTIR or UV-vis spectra but causes prevalence of PS peaks. Similarly, this study observed that the conjugates' C=O/Ti–OH groups are masked, likely due to the dominant C=C peak of PS at 1671 cm^{-1}. This suggests that the porphyrins, TiO_2, and their conjugates retain their original structure and are uniformly distributed within the PS matrix. As a result, they are likely to maintain their photosensitization properties during aPDI.[38]

3.2 X-ray diffraction (XRD)

XRD is an analytical tool used to identify the crystal structure of materials, which is essential for understanding their photocatalytic properties. Different crystal structures can significantly impact a material's photoinactivation efficiency.[39] High crystallinity of a material in photocatalysis is normally attributed to high photocatalytic activity.[40] In this study, XRD analysis were investigated to inspect the crystal properties of the nanoparticles, as well as the effect of porphyrin on the crystal structure of TiO_2. Fig. S1 confirms the amorphous nature of **1** and **2**. The XRD patterns of the nanoparticles and conjugates are shown in Fig. 2. TP and TJ showed diffraction peaks (JCPDS 00-001-0562) at 25.5, 38.3, 48.3, 54.2, 55.1, 62.9, 69.3, 70.4, and 75.6° 2θ, confirming anatase TiO_2.[41] Moreover, there were no changes in the peaks of TiO_2 when conjugated to **1** as shown in the diffraction patterns of **1**-TP and **1**-TJ. This suggests that the porphyrin had no significant influence on the crystal structure of the TiO_2 nanoparticles.[18]

3.3 Thermogravimetric analysis (TGA)

Thermogravimetric analysis was used to study the stability of the synthesized molecules. As observed, the thermograms (Fig. 3) of the porphyrins alone indicate a significant gradual percentage loss of the porphyrin molecules up to 45 and 50 °C for **1** and **2** at 900 °C, respectively. However, the TiO_2 nanoparticles alone show great thermal stability up until 900 °C, with just less than 4% weight loss due to absorbed water molecules. The conjugates, although with a slightly lower stability than

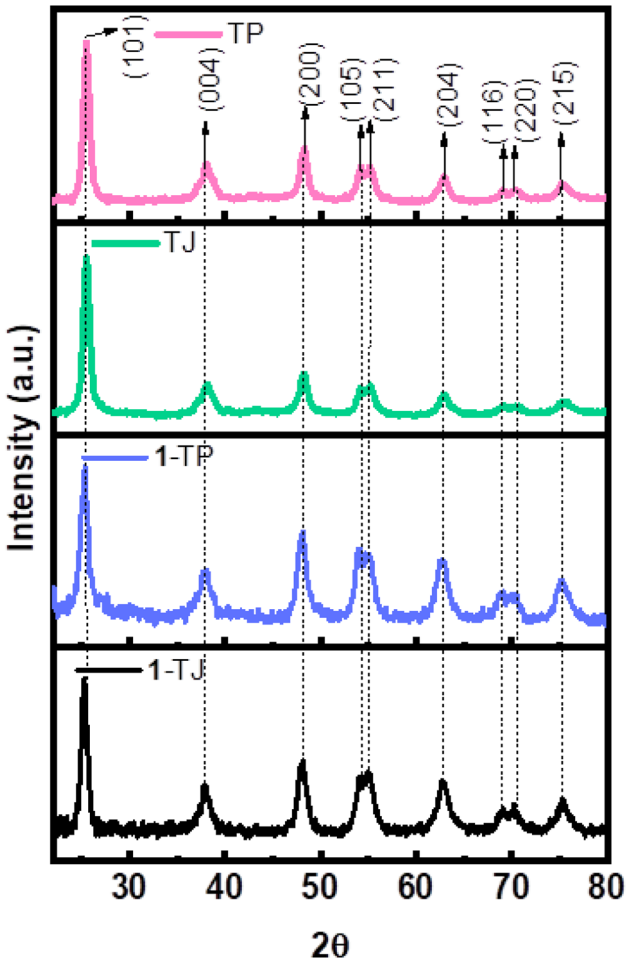

Fig. 2 XRD patterns of TP, TJ, **1**-TP, and **1**-TJ as an example.

TiO_2, show improved thermal stability (12, 7, 5, and 5% weight loss at 900 °C for **2**-TP, **2**-TJ, **1**-TP and **1**-TJ, respectively) compared to the porphyrins.

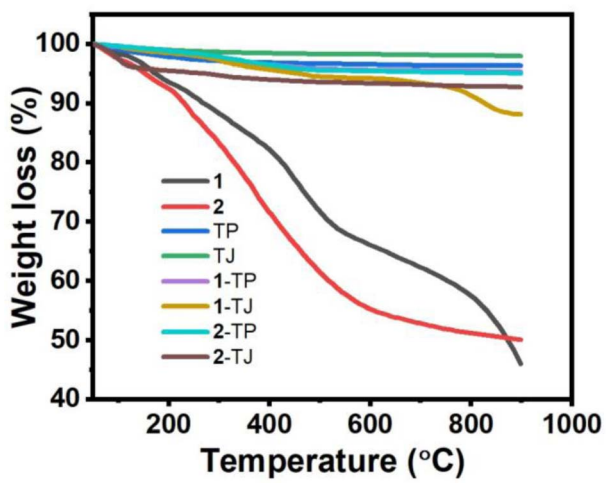

Fig. 3 TGA thermograms grams for **1**, **2**, TP, TJ, **1**-TP, **1**-TJ, **2**-TP and **2**-TJ.

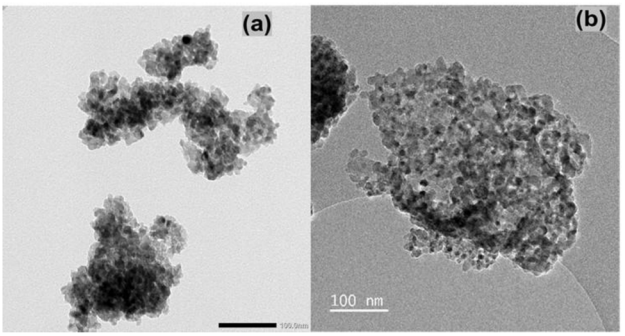

Fig. 4 TEM micrograms for TJ (a) and **2**-TJ as examples (b).

3.4 Transmission electron microscopy (TEM)

TEM was used to study the morphological analysis of the synthesized materials. Fig. 4 shows the TEM micrograms of TJ and **2**-TJ as examples. It was observed that TJ has a spherical morphology which is aggregated when in combination with porphyrin. The average sizes were calculated using image-J software and were found to be 13.71 and 13.27 nm TP and TJ, respectively. These sizes increased slightly during conjugation to 15.03, 17.30, 17.44, and 18.21 for **1**-TP, **1**-TJ, **2**-TP, and **2**-TJ, respectively. This observation was anticipated, as it aligns with the expected interaction between the porphyrin molecules and the nanoparticles, leading to a subtle alteration in their morphology.[19,42] However, the aggregation may also be due to the sample preparation method during the TEM analysis.[43]

3.5 Scanning electron microscopy (SEM)

SEM was used to examine the produced nanomaterials' morphology. Research has revealed that the shape and size of nanomaterials are influenced by the synthetic route and play a role in the efficiency of the material.[44] As observed (Fig. S1), the TJ and **2**-TJ confirmed the agglomerated spherical morphology of the free materials as observed in TEM. Fig. 5(a–

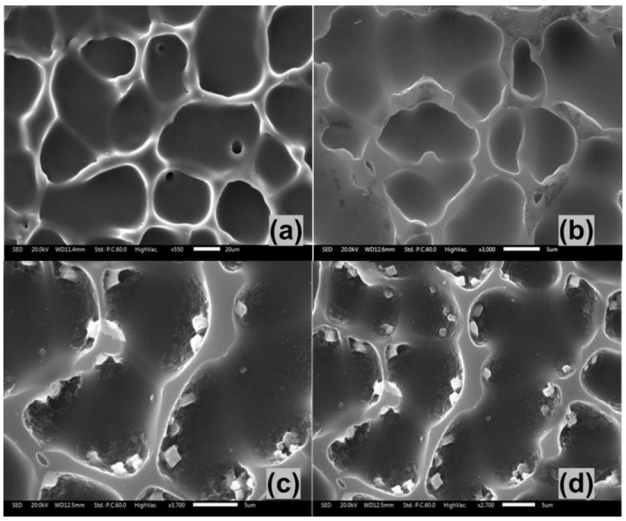

Fig. 5 SEM micrograms for PS (a), **2**-PS (b), TJ-PS (c), and **2**-TJ-PS (d) as examples.

d) shows the SEM images of the porphyrins, TiO_2 nanoparticles and conjugates immobilized onto expanded porphyrin. PS (a), 2-PS (b), TJ-PS (c), and 2-TJ-PS were used as examples. The images of the immobilized materials show porous microvoid PS with a clear presence of the nanoparticles on the surface, confirming successful immobilization. The nanoparticles are exposed on the surface of PS, which maximises the amount of light they can receive during aPDI.

3.6 Energy dispersive X-ray spectroscopy (EDX)

The elemental composition of the synthesized materials was studied using the EDX. Fig. S2 shows the EDX spectra of the free materials TP, TJ, 2-TP and 2-TJ. The elements observed are Ti, O, C, Br, In, C and Cl as expected for 2-TP and 2-TJ. The Au is due to the gold coating used during sample preparation for analysis. Furthermore, the EDX spectra of the immobilized materials (Fig. 6) confirmed the presence of all expected elements as described above for the pristine materials. This is accompanied by a strong intense carbon (C) peak which is typical for carbonous polymers.

3.7 UV-vis spectrophotometry

This study employed UV-vis spectrophotometry to investigate the light absorbance of synthesized materials. Fig. 7 shows the absorbance of TP, 1-TP, as well as 2-TP as examples. The absorption of TP is in the UV range as expected due to large bandgap energy. However, the incorporation of porphyrin onto TiO_2 nanoparticles resulted in an additional peak in the visible range, indicating successful adsorption. The strong intense

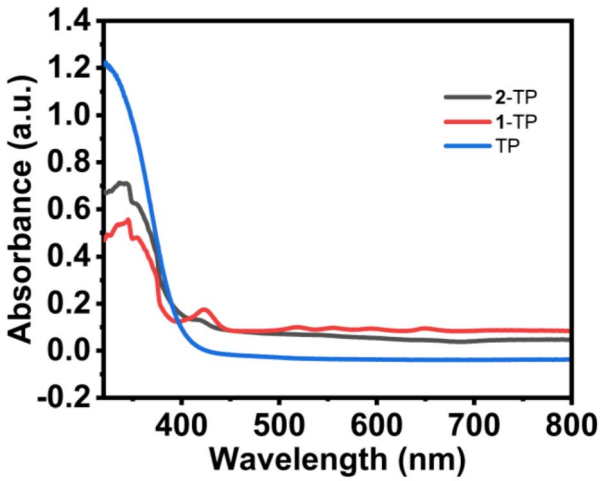

Fig. 7 Solid-state UV-vis absorption spectra of TP, 1-TP and 2-TP.

Soret band of 1 was previously found to lie at 418 nm, and that of the metalated 2 at 428 nm.[15] In this study, the Soret band of the unmetalated porphyrin conjugate 1-TP was observed at the same wavelength as its unconjugated counterpart (1, 418 nm). There was a 4-unit red shift to 424 nm for 2-TP, attributed to the interaction between TiO_2 and porphyrin. The results align with previous reports on interaction of porphyrin-TiO_2 conjugates.[13]

3.8 Photophysical properties

3.8.1 Fluorescence emission spectra. Fluorescence emission spectra measurements were performed in DMF, exciting at

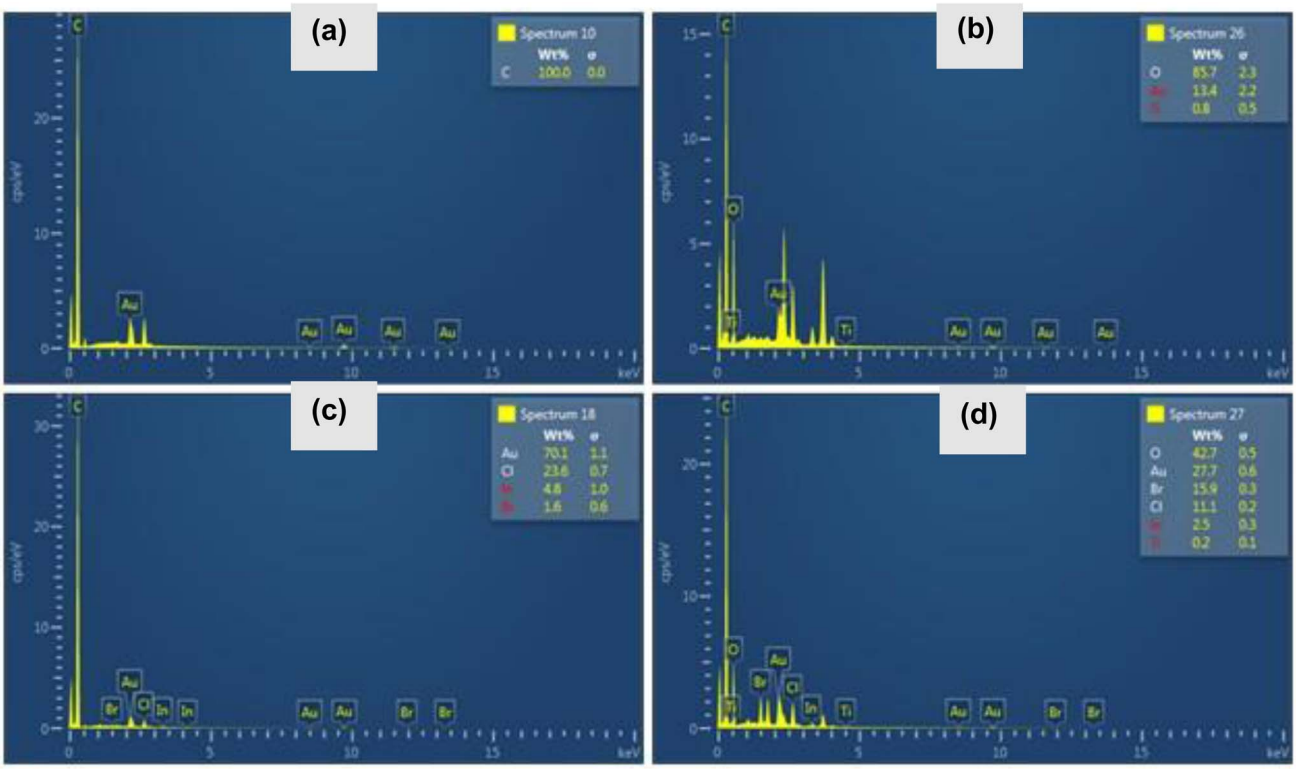

Fig. 6 EDX spectra of PS (a), TP- PS (b), 2-PS (c), and 2-TP-PS (d) as examples.

430 nm. Fig. 8a and b show the S1 → S0 fluorescence of **1**, **2**, **1**-TJ, and **2**-TJ which exhibit distinct differences in their emission profiles. All the complexes show two typical fluorescence peaks of porphyrins.[45] The metal-free porphyrin **1** displayed strong intense peaks around 660 nm for $Q(0,0)$, accompanied by secondary peak of lower intensity at around 725 and 722 nm for $Q(0,1)$ for **1** and **2**, respectively.[46] In contrast, there was an observed blue-shift in the emission profile of **2** with peaks appearing at 622 nm (strong intense) and 676 nm (less intense). This differences in the emission wavelengths may be due to the substantial change in the electronic structure and photophysical properties of the porphyrin macrocycle, likely due to the influence of the indium metal centre on the ligand's excited-state dynamics.

The fluorescence emission profiles of the conjugates are demonstrated in Fig. 8b using **1**-TJ and **2**-TJ as examples. The spectra still showed the two characteristic peaks as in the case of the porphyrins alone, however, the low intense peak for **2**-TJ appeared to have even lower intensity. The characteristic high and less intense peaks were observed at 652 and 716 nm for **1**-TJ and at 776 and 728 nm for **2**-TJ, respectively.

3.8.2 Fluorescence quantum yield (Φ_F) and lifetime (τ_F). When porphyrins' electrons get excited, they can either undergo intersystem crossing or go back to ground state through emission. Φ_F is a measure of the efficiency of the molecule to emit light through fluorescence.[26] Whereas τ_F is the average time that a molecule spends in its excited state before it relaxes and returns to ground state through photon emission. The fluorescence decay curves (Fig. S3) and τ_F of the synthesized materials were determined using time-correlated single photon counting (TCSPC). In this study, Φ_F of **1** in Table 1 was measured to be 0.01 and τ_F being 5.78 ns, these values decrease upon introduction of the indium metal, with Φ_F being <0.01 and τ_F being 3.78 ns. This effect is due to the ability of In heavy metal to stabilize the excited state, thus quenching fluorescence and promoting intersystem crossing.[45] Furthermore, conjugation caused a slight increase in the Φ_F of the conjugates with **1**, achieving 0.02 and 0.022 for **1**-TP and **1**-TJ, respectively. However, there was a decrease in the Φ_F of the conjugates with **2** as expected. On the other hand, the values of the τ_F decreased for all conjugates with the lowest Φ_F (0.001) observed for both **2**-TP and **2**-TJ and lowest τ_F (1.19 ns) observed for **2**-TJ. The values, however, were lower than what has been reported on Φ_F of TiO_2 alone (0.20) from 330–370 nm in an alcoholic medium.[47]

3.8.3 Singlet oxygen quantum yield (Φ_Δ). At the excited triplet state, when porphyrin transfers its energy to ground state molecular oxygen it produces singlet oxygen.[23] In aPDI, the aim is to have photosensitizers that produce Φ_Δ enough to inactivate bacteria in a short space of time.[6] The Φ_Δ was determined using a standard solution of TPP and ZnTPP in DMF as a reference. The Φ_Δ for **1** and **2** were reported to be 0.68 and 0.83, respectively, using TCSPC on burst mode. This confirms that indium induces heavy atom effect that improves the production of reactive oxygen species. In the conjugated materials, higher Φ_Δ were observed, the highest achieved was with the **2**-TP conjugate showing a value of 0.90. These values were higher than what has been reported on Φ_Δ of TiO_2 alone (0.12–0.38).[13,48] This improvement is desirable for light activated reactions. Fig. S4 shows the phosphorescence decay curve for the determination of Φ_Δ of **2** as an example.

Table 1 Photophysical parameters of the synthesized materials

Material	τ_F (ns)	Φ_F	Φ_Δ (±0.01)
1	5.78	0.01	0.68
2	3.78	<0.01	0.83
1-TP	1.96	0.02	0.74
1-TJ	2.13	0.022	0.74
2-TP	1.37	0.001	0.90
2-TJ	1.19	0.001	0.89

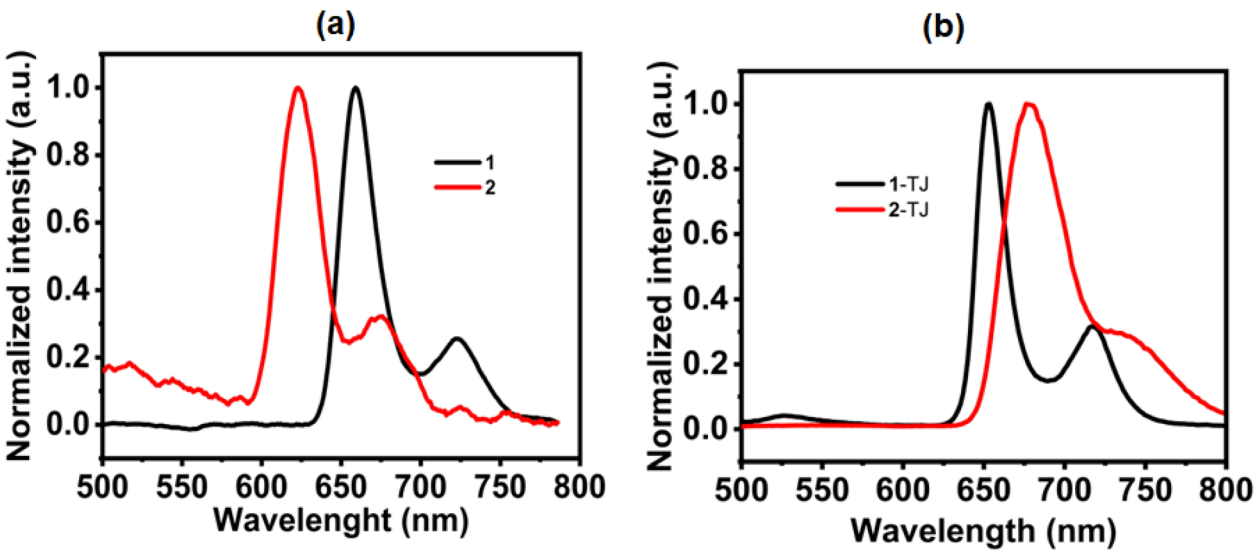

Fig. 8 Fluorescence emission spectra of **1** and **2** (a), and (b) **1**-TJ and **2**-TJ as an example for the conjugates.

3.9 Antimicrobial studies

3.9.1 Physical parameters of the pond water sample and presumptive *S. aureus* characteristics. Water samples, collected from the University of South Africa's Florida Campus, were analysed on-site for physical parameters (Table 2), revealing temperature, pH, conductivity, total dissolved solids, and turbidity levels all fell within WHO drinking water standards, yet harboured viable *S. aureus*. Fig. 9a shows positive results for presumptive *S. aureus* on mannitol salt agar plate, characterised by a golden yellow colour and colour changes of the mannitol salt agar from red to yellowish orange (mannitol fermentation). The gram staining results (Fig. 9b) showed that the bacteria were Gram positive and cocci shaped in single and even paired in chains. Fig. 9c revealed a positive catalase test of the bacteria indicated by the presence of bubbles. All the morphological characterization and catalase test matched *S. aureus*.

3.9.2 Gel electrophoresis and CF-01 sanger sequencing results. Gel electrophoresis is a technique that used for separating molecules by size and charge using an electric field.[49] It is used to separate DNA, RNA, or proteins. In this study, DNA extraction was conducted, followed by PCR, and gel-electrophoresis was then employed to separate PCR amplicons of *S. aureus* samples. Fig. 10 shows the results from gel electrophoresis which indicate that the DNA was present, and that PCR was successful. No contamination was observed in the samples. Furthermore, the data matched the 16S rRNA gene with a band at 1500 base pairs.[50]

The 16S rRNA Sanger sequencing results (Fig. 11) confirmed that the isolated presumptive bacteria were indeed *S. aureus*. The results were analysed using Geneious prime software. All the top hit results from NCBI BAST analysis, when compared to the submitted DNA query sequence, matched S. *aureus.* The query coverage and percentage identity for all the isolates after NCBI BAST analysis were 100% (Table 3) indicating a strong match between the query sequences and matched one in the NCBI. All the query sequences had the expected value (*E* value) of zero, indicating good quality of sequencing alignment. The 16S rRNA Sanger sequencing results confirmed that the isolated bacteria were *S. aureus*.

3.9.3 aPDI results in suspended bacteria using free photosensitizers. All the aPDI experiments were performed using in photosensitizer materials suspended in PBS. For assurance, validation, and reliability of the results, aPDI studies were conducted in triplicates. Environmental *S. aureus* was employed as Gram-positive bacteria to study the aPDI activity of the synthesized materials. A lower survival percentage after light exposure indicates the photosensitizer's higher efficacy. This study investigated the antimicrobial activity of metal-free (**1**) and indium(III) porphyrin (**2**) conjugates with titanium dioxide nanoparticles synthesized from orange-peel extract (TP) and orange juice (TJ).

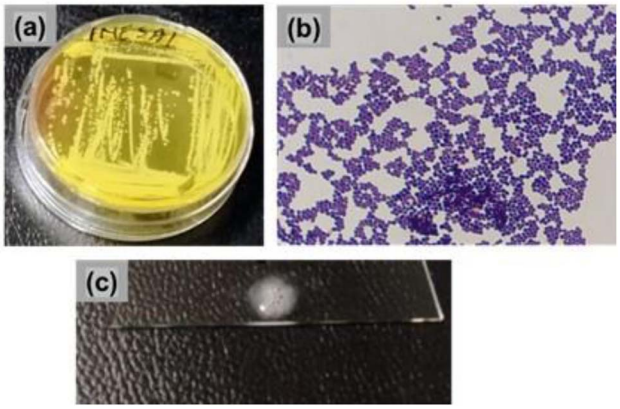

Fig. 9 Presumptive *S. aureus* colonies on mannitol salt agar after steaking and incubating for 24 hours at 37 °C (a), presumptive *S. aureus* gram staining results viewed under Olympus CX23 microscopy at 100× oil objective (b), and catalase test results of presumptive *S. aureus* (c).

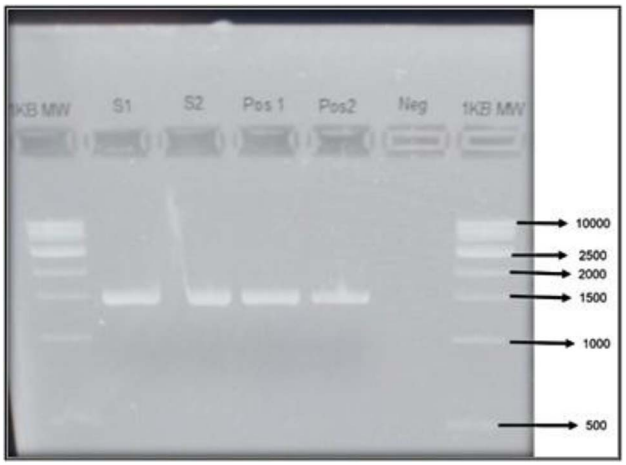

Fig. 10 Gel electrophoresis results. 1 KB MW is the 1 kb DNA ladder, 1% agarose, 1xTEA used, S1 and S2 are the DNA amplicons samples in duplicates, Pos2 and Neg are the positive and negative controls (*S. aureus*). The numbers on the right represent the base pairs.

The bacterial suspensions in PBS without any photosensitizer were used as controls. The photosensitizers showed negligible dark toxicity (Fig. S5) at concentration from (0.05–1.00 mg mL^{-1}). Concentration optimization under light revealed 0.25 mg mL^{-1} as optimal as lower and higher concentrations showed lower efficiency. This fixed concentration was used for systematic time-dependent comparison studies (Fig. 12 and Table 4).

Table 2 Physical parameters of the water samples collected at a pond at UNISA, Florida campus

Site name	Temperature (°C)	pH	Conductivity	Total dissolved solids (ppm)	Turbidity
Pond water	13.5 ± 0.5	8.29 ± 0.2	833 ± 3.2	418 ± 1.9	0.00 ± 0.0

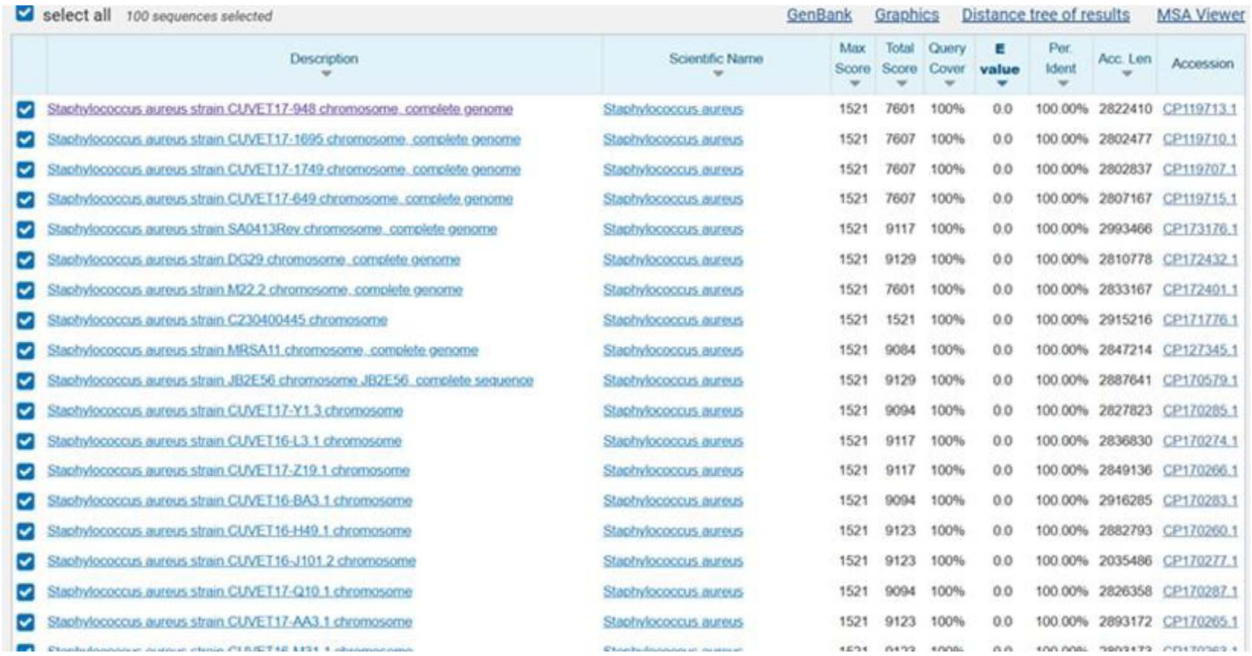

select all 100 sequences selected GenBank Graphics Distance tree of results MSA Viewer

Description	Scientific Name	Max Score	Total Score	Query Cover	E value	Per. Ident	Acc. Len	Accession
Staphylococcus aureus strain CUVET17-948 chromosome, complete genome	Staphylococcus aureus	1521	7601	100%	0.0	100.00%	2822410	CP119713.1
Staphylococcus aureus strain CUVET17-1695 chromosome, complete genome	Staphylococcus aureus	1521	7607	100%	0.0	100.00%	2802477	CP119710.1
Staphylococcus aureus strain CUVET17-1749 chromosome, complete genome	Staphylococcus aureus	1521	7607	100%	0.0	100.00%	2802837	CP119707.1
Staphylococcus aureus strain CUVET17-649 chromosome, complete genome	Staphylococcus aureus	1521	7607	100%	0.0	100.00%	2807167	CP119715.1
Staphylococcus aureus strain SA0413Rev chromosome, complete genome	Staphylococcus aureus	1521	9117	100%	0.0	100.00%	2993466	CP173176.1
Staphylococcus aureus strain DG29 chromosome, complete genome	Staphylococcus aureus	1521	9129	100%	0.0	100.00%	2810778	CP172432.1
Staphylococcus aureus strain M22.2 chromosome, complete genome	Staphylococcus aureus	1521	7601	100%	0.0	100.00%	2833167	CP172401.1
Staphylococcus aureus strain C230400445 chromosome	Staphylococcus aureus	1521	1521	100%	0.0	100.00%	2915216	CP171776.1
Staphylococcus aureus strain MRSA11 chromosome, complete genome	Staphylococcus aureus	1521	9084	100%	0.0	100.00%	2847214	CP127345.1
Staphylococcus aureus strain JB2E56 chromosome JB2E56, complete sequence	Staphylococcus aureus	1521	9129	100%	0.0	100.00%	2887641	CP170579.1
Staphylococcus aureus strain CUVET17-Y1.3 chromosome	Staphylococcus aureus	1521	9094	100%	0.0	100.00%	2827823	CP170285.1
Staphylococcus aureus strain CUVET16-L3.1 chromosome	Staphylococcus aureus	1521	9117	100%	0.0	100.00%	2836830	CP170274.1
Staphylococcus aureus strain CUVET17-Z19.1 chromosome	Staphylococcus aureus	1521	9117	100%	0.0	100.00%	2849136	CP170266.1
Staphylococcus aureus strain CUVET16-BA3.1 chromosome	Staphylococcus aureus	1521	9094	100%	0.0	100.00%	2916285	CP170283.1
Staphylococcus aureus strain CUVET16-H49.1 chromosome	Staphylococcus aureus	1521	9123	100%	0.0	100.00%	2882793	CP170260.1
Staphylococcus aureus strain CUVET16-J101.2 chromosome	Staphylococcus aureus	1521	9123	100%	0.0	100.00%	2035486	CP170277.1
Staphylococcus aureus strain CUVET17-Q10.1 chromosome	Staphylococcus aureus	1521	9094	100%	0.0	100.00%	2826358	CP170287.1
Staphylococcus aureus strain CUVET17-AA3.1 chromosome	Staphylococcus aureus	1521	9123	100%	0.0	100.00%	2893172	CP170265.1

Fig. 11 CF-01 Sanger sequencing results.

Table 3 Presumptive and sanger sequencing results obtained for the *S. aureus* used in this study

Sample	Presumptive bacteria	Identified bacteria	Query coverage	% Identity	Expected value
1	*S. aureus*	*S. aureus*	100%	100	0

Notably, the control alone without the photosensitizer did not cause any significant reduction in the survival percentage of the bacteria in both the dark and light experiments. However, the porphyrins **1** and **2** reduced *S. aureus* survival, up to approximately 20% after exposure to LED light. Notably, porphyrin **2** performed better than **1** alone as expected due to

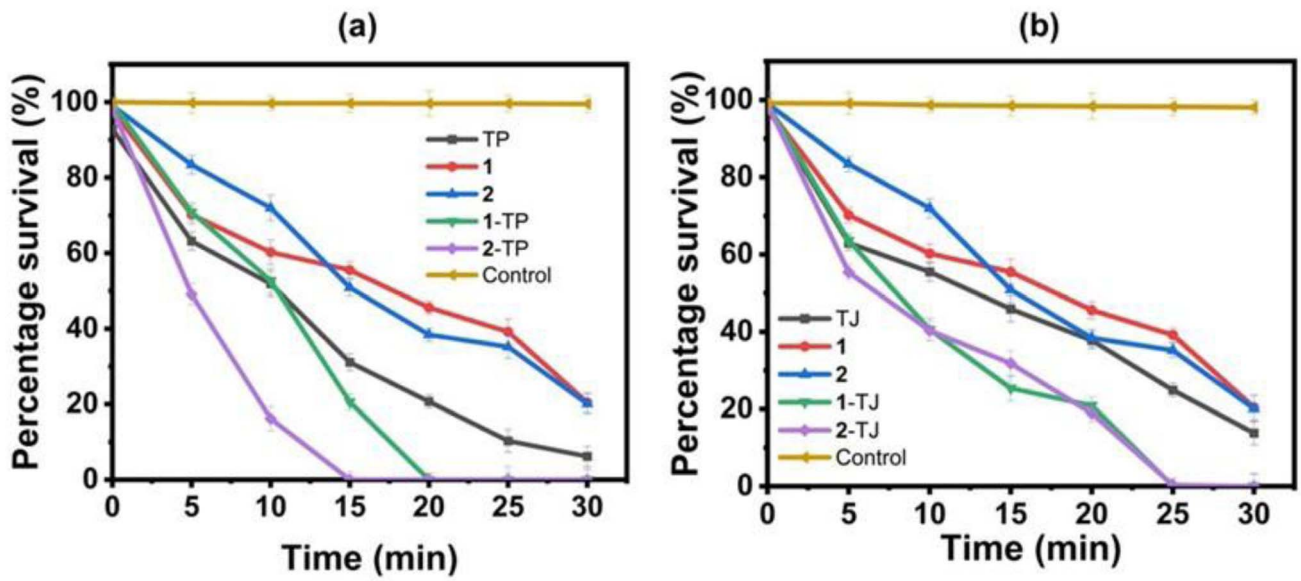

Fig. 12 aPDI results studies using TP, **1**, **2**, **1**-TP, **2**-TP (a) and TJ, **1**, **2**, **1**-TJ, **2**-TJ (b) against *S. aureus* in PBS suspension. The experiments were conducted for 30 minutes with 5 minutes sampling intervals under light and control experiments were done using the bacteria only, without any photosensitizer.

Table 4 Survival percentages of freely suspended *S. aureus* after photoinactivation using TP, **1**, **2**, **1**-TP, **2**-TP, TJ, **1**-TJ, and **2**-TJ. The experiments were conducted for 30 minutes with 5 minutes sampling intervals under light and control experiments were done using the bacteria only, without any photosensitizer

Time (min)	TP	**1**	**2**	**1**-TP	**2**-TP	Control	TJ	**1**-TJ	**2**-TJ
0	97.9 ± 1.95	98.0 ± 1.93	99.1 ± 1.96	99.1 ± 1.94	98.2 ± 1.90	99.2 ± 3.21	97.9 ± 3.78	98.9 ± 3.66	98.8 ± 2.84
5	63.2 ± 2.42	70.23 ± 2.48	83.4 ± 2.44	70.9 ± 2.50	49.1 ± 2.84	99.1 ± 2.76	63 ± 3.98	63.6 ± 1.93	55.4 ± 2.00
10	51.9 ± 3.38	60.22 ± 3.27	71.99 ± 3.39	52.7 ± 3.28	16.2 ± 3.26	98.7 ± 1.98	55.5 ± 2.56	50.6 ± 2.90	40.3 ± 2.53
15	31.1 ± 2.21	55.5 ± 2.13	50.9 ± 2.23	20.6 ± 2.15	0.022 ± 0.04	98.5 ± 2.46	45.9 ± 3.35	35.4 ± 3.32	31.8 ± 3.41
20	20.7 ± 1.78	45.6 ± 1.75	38.4 ± 1.79	0.009 ± 0.01	0.006 ± 0.00	98.4 ± 3.41	37.8 ± 2.22	20.9 ± 2.16	18.9 ± 3.31
25	10.3 ± 3.05	39.2 ± 3.42	35.2 ± 3.06	0.003 ± 0.00	0.001 ± 0.00	98.3 ± 2.24	24.9 ± 1.18	0.07 ± 0.02	0.3 ± 0.10
30	6.2 ± 2.65	20.43 ± 2.59	20.1 ± 2.67	0.001 ± 0.00	0.0006 ± 0.00	98.1 ± 2.23	13.8 ± 1.09	0.03 ± 0.01	0.01 ± 0.00

the heavy atom effect of the indium that assists in promoting intersystem crossing during the photoinactivation.[51] The nanoparticles TP and TJ show comparatively better antimicrobial activity with TP performing better than TJ. The reason behind this is unclear, however, it may be due distinct phytochemical profiles, pH, sugar content, and viscosity of the extracts, affecting reduction kinetics, particle size, and surface capping.

The conjugates, **1**-TP, **2**-TP, **1**-TJ and **2**-TJ were observed to cause significant reduction of bacteria. **2**-TP caused almost complete inactivation of *S. aureus* after just 15 min, while **2**-TJ achieved this after 25 minutes. The highest reduction in the survival percentage (0.0004%) was observed with the **2**-TP

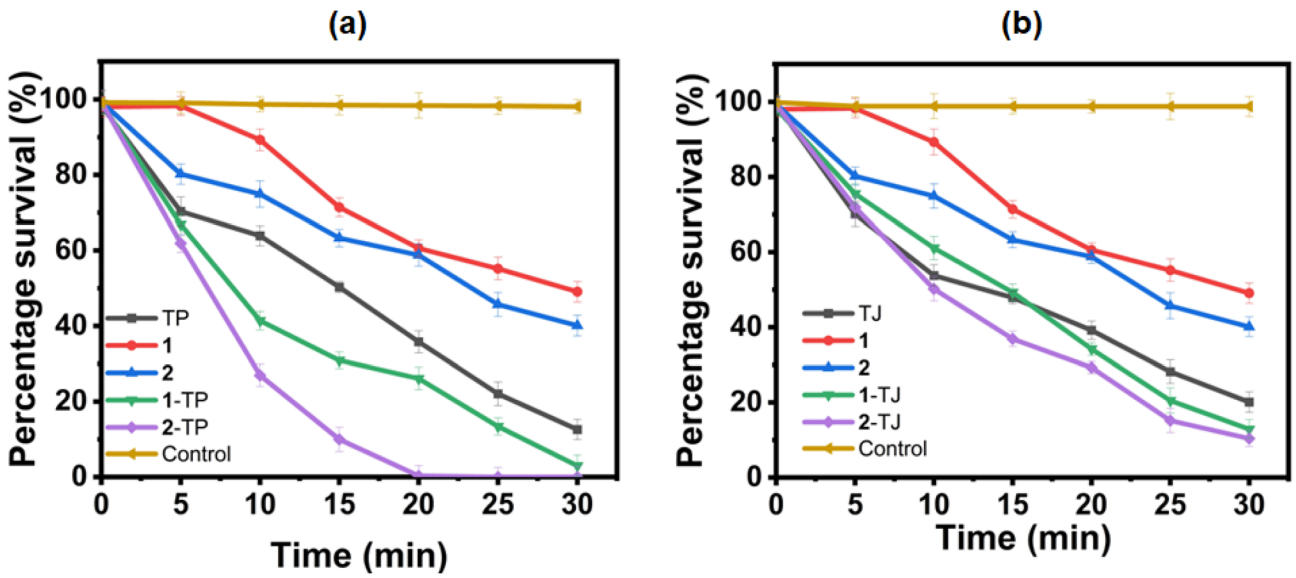

Fig. 13 aPDI results studies using TP, **1**, **2**, **1**-TP, **2**-TP (a) and TJ, **1**, **2**, **1**-TJ, **2**-TJ (b) against biofilm *S. aureus*. The experiments were conducted for 30 minutes with 5 minutes sampling intervals under light and control experiments were done using the biofilm bacteria only, without any photosensitizer.

Table 5 Survival percentages of biofilm *S. aureus* after photoinactivation using TP, **1**, **2**, **1**-TP, **2**-TP, TJ, **1**-TJ, and **2**-TJ. The experiments were conducted for 30 minutes with 5 minutes sampling intervals under light and control experiments were done using the biofilm *S. aureus* only, without any photosensitizer

Time (min)	TP	**1**	**2**	**1**-TP	**2**-TP	Control	TJ	**1**-TJ	**2**-TJ	Control
0	98.3 ± 2.28	98.0 ± 2.70	99.4 ± 3.16	99.0 ± 2.61	99.5 ± 2.61	99.2 ± 3.17	99.0 ± 2.18	98.2 ± 1.89	99.2 ± 1.86	99.9 ± 1.95
5	70.3 ± 3.82	98.3 ± 2.53	80.2 ± 2.69	66.9 ± 2.87	61.9 ± 2.42	99.1 ± 2.82	70.1 ± 3.26	75.5 ± 2.54	71.9 ± 2.81	99.4 ± 2.41
10	63.9 ± 2.65	89.3 ± 2.87	74.9 ± 3.50	41.4 ± 2.44	26.97 ± 2.93	98.7 ± 2.00	53.8 ± 2.85	61.1 ± 3.08	50.2 ± 3.23	99.2 ± 3.29
15	50.3 ± 1.40	71.4 ± 2.45	63.3 ± 2.27	30.9 ± 2.15	10 ± 3.20	98.5 ± 2.60	47.9 ± 1.64	49.3 ± 2.25	56.9 ± 2.06	98.7 ± 2.13
20	35.8 ± 2.92	60.6 ± 2.23	58.8 ± 2.94	26.1 ± 2.98	0.32 ± 0.05	98.4 ± 3.38	39.2 ± 2.47	34.2 ± 1.71	29.3 ± 1.59	98.4 ± 1.74
25	22.07 ± 3.17	55.2 ± 2.99	45.7 ± 3.19	13.4 ± 2.28	0.02 ± 0.00	98.3 ± 2.27	28.2 ± 3.13	20.5 ± 3.35	15.2 ± 3.19	98.3 ± 3.46
30	12.6 ± 2.70	49.1 ± 2.70	40.1 ± 2.73	3 ± 0.83	0.004 ± 0.00	98.2 ± 1.85	20.1 ± 2.71	12.9 ± 2.49	10.4 ± 2.16	98.1 ± 2.62

conjugates after 30 minutes indicating a strong interaction between the indium metalated porphyrin and the nanoparticles. This superiority directly correlates with **2**-TP's optimized photophysical parameters, where both heavy atom effect quenching and porphyrin electron transfer to TiO_2 maximizes triplet population and singlet oxygen production.[15]

The results suggest that the survival percentage is inversely proportional to the irradiation time. Moreover, conjugation with TiO_2 increases the antibacterial activity.

3.9.4 aPDI results for antibiofilm studies using free photosensitizers. Biofilms are complex communities of bacteria enclosed in a protective matrix, making them resistant to antimicrobial treatments. For this reason, a higher photosensitizer concentration (0.50 mg mL^{-1}) than that used in the planktonic bacteria was found to be optimal (Fig. S5). The results in Fig. 13 and Table 5 showed that the porphyrins significantly inhibited biofilm growth, with survival percentages as low as 49.1% and 40.1% for **1** and **2**, respectively. These values are better than what has been previously reported with porphyrins such as TAPP and TCPP which inhibited *S. aureus* biofilms by 37% and 48%.[52] Notably, *S. aureus*, with its single membrane layer, is known to be comparably susceptible to the antibacterial effects. The porphyrins likely inhibit bacterial cell metabolism, damage the cytoplasmic membrane, and increase cell permeability.[28]

Biofilms are known to be difficult to inactivate as the ROS first needs to pass through the EPS matrix to rich the target bacteria. This explains the slightly reduced efficiency of the photosensitizers against biofilms as compared to the bacteria in their freely forms. Nevertheless, the results demonstrated that the conjugates derived from TP exhibited higher efficiency in eradicating biofilms compared to those synthesized from TJ, complementing the results from freely suspended bacteria. Further investigation is needed to elucidate the specific mechanisms underlying the enhanced antibiofilm activity of TP conjugates. The best performing photosensitizer, **2**-TP, achieved almost complete reduction of biofilm *S. aureus* after 20 min, which is longer than what was achieved using the same photosensitizer to inactivate freely suspended bacteria, which required only 15 minutes to achieve the same effect.

3.9.5 Photoinactivation of freely suspended bacteria using immobilized photosensitizers. The synthesized **1** and **2**, TiO_2 nanoparticles, as well as their corresponding conjugates immobilized onto waste PS were tested for photodynamic activity. PS support allows for ease of separation of the photosensitizer after use. The test microorganism was still the same, environmental *S. aureus*, in both suspension and biofilm. Control experiments with the bacterial suspension but without a photosensitizer, and with the photosensitizers in the dark, showed essentially no significant photodynamic effect.

PS is a polymer that has been found not to cause inhibition against *S. aureus*.[23] Hence, in this study, PS alone (Table 6) showed no significant change in the survival percentage of the bacteria. The trend in the efficiency of the photosensitizers is almost the same in their free, as well as immobilized forms. Notably, the photosensitizers immobilized onto PS were found to have a slightly reduced antimicrobial activity compared to the photosensitizers in their free forms as expected. For example,

Table 6 Survival percentages of freely suspended *S. aureus* after photoinactivation using PS immobilized photosensitizers TP-PS, **1**-PS, **2**-PS, **1**-TP-PS, **2**-TP-PS, TJ-PS, **1**-TJ-PS, and **2**-TJ-PS. The experiments were conducted for 30 minutes with 5 minutes sampling intervals under light and control experiments were done using the bacteria only, without any photosensitizer

Time (min)	TP-PS	**1**-PS	2-PS	1-TP-PS	2-TP-PS	Control	TJ-PS	**1**-TJ-PS	2-TJ-PS	PS	Control
0	99.9 ± 3.12	99.3 ± 3.00	99.6 ± 3.27	99.3 ± 3.65	99.0 ± 3.67	99.4 ± 3.69	99.7 ± 3.01	99.8 ± 1.87	99.8 ± 2.25	98.1 ± 3.33	98.9 ± 2.86
5	79.3 ± 2.67	98.9 ± 3.04	89.3 ± 2.23	74.6 ± 2.05	99.2 ± 2.83	99.4 ± 2.78	70.8 ± 2.34	69.3 ± 2.86	60.3 ± 2.09	97.8 ± 4.64	98.5 ± 2.75
10	76.1 ± 2.32	90.2 ± 4.21	82.9 ± 2.01	53.8 ± 2.77	32.3 ± 3.29	99.3 ± 3.33	66.9 ± 3.35	51.9 ± 3.12	49.1 ± 3.10	97.7 ± 2.74	98.3 ± 3.54
15	59.9 ± 2.34	83.3 ± 2.39	74.1 ± 2.96	36.9 ± 2.96	21.4 ± 2.01	99.1 ± 3.23	64.6 ± 3.82	43.5 ± 2.22	38.9 ± 2.00	97.5 ± 3.63	98.2 ± 2.55
20	41.5 ± 3.00	72.7 ± 2.88	62.9 ± 3.47	24.1 ± 3.05	4.9 ± 1.21	98.9 ± 3.76	52.8 ± 1.66	31.3 ± 3.54	24.8 ± 3.50	97.33 ± 2.43	98.2 ± 1.87
25	31.7 ± 2.23	60.8 ± 1.67	56.8 ± 1.37	17.5 ± 1.32	0.01 ± 0.01	98.5 ± 2.26	43.3 ± 1.56	20.9 ± 2.77	8.2 ± 0.90	97.1 ± 3.44	97.8 ± 1.34
30	29.8 ± 1.97	58.2 ± 2.98	51.1 ± 2.14	9.3 ± 1.19	0.006 ± 0.00	98.5 ± 2.45	31.9 ± 1.06	7.9 ± 1.11	0.04 ± 0.01	96.1 ± 1.34	97.6 ± 2.86

Table 7 Survival percentages of biofilm *S. aureus* after photoinactivation using PS immobilized photosensitizers TP-PS, **1**-PS, **2**-PS, **1**-TP-PS, **2**-TP-PS, TJ-PS, **1**-TJ-PS, and **2**-TJ-PS. The experiments were conducted for 30 minutes with 5 minutes sampling intervals under light and control experiments were done using biofilm *S. aureus* only, without any photosensitizer

Time (min)	TP-PS	**1**-PS	**2**-PS	**1**-TP-PS	**2**-TP-PS	Control	TJ-PS	**1**-TJ-PS	**2**-TJ-PS	PS	Control
0	99.4 ± 3.39	98.6 ± 3.54	99.2 ± 3.46	99.3 ± 3.95	99.8 ± 3.33	99.6 ± 3.97	99.5 ± 3.34	99.9 ± 2.29	98.9 ± 3.42	99.8 ± 3.21	99.9 ± 3.17
5	86.9 ± 3.41	98.2 ± 2.89	93.3 ± 3.68	78.4 ± 2.65	71.1 ± 2.87	99.4 ± 3.20	90.2 ± 1.18	82.5 ± 1.87	74.9 ± 3.33	98.5 ± 3.12	99.8 ± 2.82
10	76.3 ± 2.90	94.3 ± 2.05	83.1 ± 2.65	64.7 ± 3.33	58.3 ± 1.98	99.2 ± 2.09	78.3 ± 1.99	68.4 ± 1.68	61.2 ± 2.58	98.2 ± 4.00	99.6 ± 2.00
15	50.3 ± 2.06	80.5 ± 3.00	76.9 ± 2.51	54.4 ± 3.19	39.5 ± 1.76	98.7 ± 2.99	67.4 ± 2.76	56.6 ± 1.44	46.9 ± 2.95	97.9 ± 3.60	99.5 ± 2.60
20	45.8 ± 1.32	69.4 ± 1.03	63.7 ± 2.55	38.8 ± 2.64	20.9 ± 1.20	98.2 ± 1.00	52.3 ± 2.37	38.9 ± 1.34	30.0 ± 3.19	97.6 ± 3.26	99.5 ± 3.38
25	39.9 ± 2.48	54.3 ± 2.28	49.1 ± 3.65	15.5 ± 1.39	3.4 ± 1.32	97.8 ± 1.68	46.5 ± 2.87	25.3 ± 1.11	21.9 ± 3.27	97.4 ± 3.81	99.5 ± 2.27
30	32.8 ± 3.49	50.4 ± 2.88	43.7 ± 2.45	2.5 ± 1.17	0.9 ± 0.04	97.5 ± 3.87	39.1 ± 2.82	10.4 ± 1.79	4.4 ± 2.70	97.3 ± 1.74	99.2 ± 1.85

only **2**-TP could cause significant bacterial reduction, achieving almost complete (0.01%) reduction in the survival percentage after 25 minutes. Notably, this was even longer than inactivation of freely suspended bacteria using free **2**-TP (almost complete survival percentage reduction after 15 minutes).

3.9.6 Photoinactivation of biofilm bacteria using immobilized photosensitizers. The photoinactivation of biofilm bacteria using immobilized photosensitizers was also investigated, with the goal of developing a more practical and reusable antimicrobial system. The results in Table 7 showed that the immobilized photosensitizers, including **1**, **2**, TP, TJ, and their conjugates, exhibited slightly reduced antibiofilm activity compared to their free forms. However, the **2**-TP conjugate immobilized on PS still achieved significant biofilm reduction, with almost complete (0.9%) inactivation of *S. aureus* biofilm after 30 minutes of light exposure. The conjugates from TJ could not cause almost complete reduction in bacterial survival percentage. However, **2**-TJ showed better efficiency, achieving 4.4% survival percentage after 30 minutes of light exposure.

This demonstrates the potential of immobilized photosensitizers for practical applications, such as coating water storage systems surfaces to prevent biofilm formation and reduce the risk of waterborne infections. While the level of antimicrobial photodynamic activity observed is not yet sufficient for practical purposes, where a 5-log kill would be desirable, with this model system, the study has demonstrated the concept that the photodynamic effect with immobilized photosensitizers can be used to lower microbial levels in water. The system might also have applications to water decontamination.

4 Conclusions

Metal-free (**1**) and indium metalated (**2**) 5,10,15-*tris*-(4-bromopheyl)-20-(4-carboxyphenyl)porphyrin conjugates with green synthesized TiO_2 nanoparticles were synthesized successfully and immobilized onto waste PS. Their photophysical behaviour was evaluated which showed that conjugates generate higher amount of singlet oxygen, thus, better photosensitizers compared to the porphyrins (**1** and **2**) alone and an indication that introduction of TiO_2 into the porphyrin improves the efficiency of porphyrin complexes as photosensitizers. Furthermore, the conjugates with TiO_2 synthesized from orange peel extract performed better than those from orange juice indicating that the different phytochemicals within the materials play a significant role in their efficiency. Antimicrobial studies revealed significant efficiency of the conjugates in their free and immobilized forms against freely suspended and biofilm *S. aureus* under light. The study demonstrated that porphyrin conjugates from green synthesized TiO_2 may have potential to be used for inactivation of biofilms in water storage systems *via* antimicrobial photodynamic inactivation.

Author contributions

N. M.: conceptualization, visualization, methodology, formal analysis, investigation, and writing—original draft. N. K. M.: methodology, investigation, writing. C. I. N.: writing – review, funding acquisition and editing. O. J. A. writing – review, funding acquisition and editing. R. M. M.: validation, project administration, writing—review and editing, supervision. M. M.: conceptualization, validation, resources, funding acquisition, project administration, writing—review and editing, supervision. All authors have read and agreed to the published version of the manuscript.

Conflicts of interest

There are no conflicts to declare.

Data availability

The data supporting this article has been included as part of the supplementary information (SI). The raw/processed data required to reproduce these findings cannot be shared at this time as the data also form part of an ongoing study. Supplementary information is available. See DOI: https://doi.org/10.1039/d6ra00069j.

Acknowledgements

This research was funded by the Royal Society through grant number ICAO/R1/231012 – International Science Partnership Fund (ISPF) – International Collaboration Awards and Institute for Nanotechnology and Water Sustainability (iNanoWS), University of South Africa (UNISA). This work was supported by the University of South Africa, Institute for Nanotechnology and Water Sustainability (iNanoWS), CSIR National Laser Centre, as

well as the Department of Science, Innovation and Technology (DSTI), South Africa through the South African Women in Science Awards (SAWiSA) DSTI-Esther Mahlangu Fellowship (Masters).

References

1 World Health Organization, *WHO Water, Sanitation, Hygiene and Waste Strategy 2026–2035*, DOI: 10.2471/B09661, accessed 21 March 2026.
2 UNESCO, The United Nations World Water Development Report 2026, *Water for All People: Equal Rights and Opportunities*, DOI: 10.54679/NXCL7067, accessed 21 March 2026.
3 M. Bonso, D. Bedada and S. Dires, Bacterial Contamination and Antimicrobial Resistance in Drinking Water From Food and Drinking Establishments in Shashemane Town , Ethiopia, *Environ. Health Insights*, 2023, **17**, 1–8.
4 X. Ren, S. Zhang, M. Wu, B. Xiao, H. Miao and H. Chen, Effect and influence mechanism of biofilm formation on the biological stability of reclaimed water, *Sci. Total Environ.*, 2024, **906**, 167735.
5 R. E. Hinna, R. Saad, A. Khan, M. Javed, Z. A. Khan and U. A. Khan, Waterborne Diseases in a Rural Community in Pakistan : Awareness , Impact , and Corrective Measures Study area and duration, *Cureus*, 2025, **17**, e93154.
6 N. Malomane, M. Mlambo, A. T. Kuvarega, R. M. Moutloali and M. Managa, *Int. J. Environ. Sci. Technol.*, 2024, **22**, 4975–5006.
7 D. Zhong, Z. Zhou, W. Ma, J. Ma, W. Feng, J. Li and X. Du, Antibiotic enhances the spread of antibiotic resistance among chlorine-resistant bacteria in drinking water distribution system, *Environ. Res.*, 2022, **211**, 113045.
8 T. Nguyen, D. Mcgiffin, B. Lou, Y. Sun, C. Qian, W. Zhang, A. Y. Peleg, Y. Qu, T. Nguyen, D. Mcgiffin, B. Lou, Y. Sun and C. Qian, Assembling the puzzle of antimicrobial resistance in staphylococcal biofilms, *Emerg. Microbes Infect.*, 2026, **15**, 1–11.
9 K. S. Ndlovu, M. J. Moloto, K. E. Sekhosana, T. T. I. Nkambule and M. Managa, Porphyrins developed for photoinactivation of microbes in wastewater, *Environ. Sci. Pollut. Res.*, 2023, **30**, 11210–11225.
10 M. Managa, T. G. T. Moraba, N. Malomane and K. Nene, A New Way to Treat Diseases Using Light-Loving Molecules, *Front. Young Minds*, 2024, **12**, 1377991.
11 M. K. Nhlabathi-Chidi, N. M. Mametja, T. T. I. Nkambule, U. Feleni, T. Masebe and M. Managa, An Overview of the Current Approaches in Drug-Resistant Bacterial Removal Within Wastewaters: Can We Move Towards Nanomagnet-Porphyrin Hybrids for Antimicrobial Photodynamic Inactivation (aPDI), *Curr. Microbiol.*, 2025, **82**, 1–16.
12 N. Bridged Magaela, L. C. Makola, M. Managa and T. Nyokong, Photodynamic activity of novel cationic porphyrins conjugated to graphene quantum dots against Staphylococcus aureus, *J. Porphyr. Phthalocyanines*, 2022, **26**, 392–402.
13 K. Hlabangwane, R. Matshitse, M. Managa and T. Nyokong, The application of Sn(IV)Cl_2 and In(III)Cl porphyrin-dyed TiO_2 nanofibers in photodynamic antimicrobial chemotherapy for bacterial inactivation in water, *Photodiagnosis Photodyn. Ther.*, 2023, **44**, 103795.
14 L. Zhao, J. Zhao, Z. Mo, Z. Wang, Z. Xue, L. Feng and L. Zhao, Pyridine-substituted zinc porphyrin/TiO_2 nanoparticles for increased light harvesting and efficient photocatalysis, *J. Mol. Struct.*, 2026, **1354**, 144949.
15 N. Malomane, R. M. Moutloali and M. Managa, Enhanced visible light degradation of indigo carmine dye using conventional and green synthesized TiO_2 conjugates with porphyrin, *J. Mol. Struct.*, 2025, **1336**, 142063.
16 A. Mobeen Amanulla and R. Sundaram, Green synthesis of TiO_2 nanoparticles using orange peel extract for antibacterial, cytotoxicity and humidity sensor applications, *Mater. Today Proc.*, 2019, **8**, 323–331.
17 A. Sułek, B. Pucelik, M. Kobielusz, P. Łabuz, G. Dubin and J. M. Dąbrowski, Surface modification of nanocrystalline TiO_2 materials with sulfonated porphyrins for visible light antimicrobial therapy, *Catalysts*, 2019, **9**, 821.
18 K. S. Min, R. S. Kumar, J. H. Lee, K. S. Kim, S. G. Lee and Y. A. Son, Synthesis of new TiO_2/porphyrin-based composites and photocatalytic studies on methylene blue degradation, *Dye. Pigment.*, 2019, **160**, 37–47.
19 Z. Li, C. Wang, Z. Su, W. Zhang, N. Wang, G. Mele and J. Li, New porphyrin/Cu(II) porphyrin-TiO_2 nanohybrids for improved photocatalytic oxidation and reduction activities, *Mater. Chem. Phys.*, 2020, **252**, 123228.
20 S. H. El-khalafy, M. T. Hassanein, N. A. Salahuddin and M. M. Alaskary, Efficient oxidative degradation of Azo dyes by cobalt(II) porphyrin complex supported on modified bentonite and chitosan : structural characterization and mechanistic insight, *Sci. Rep.*, 2025, **15**, 34282.
21 J. Liu, W. Qiu, S. Dou, H. Shang, Y. Zhang and J. Xu, Quartz wool-supported porphyrin supramolecular photocatalysts for robust and scalable H_2O_2 generation, *EES So.*, 2025, **1**, 1115–1125.
22 X. Chen, S. Zhuang, W. Yan, Z. Zeng, J. Feng and H. Cao, Synthesis , antibacterial evaluation , and safety assessment of Se@PLA as a potent bactericide against Xanthomonas oryzae pv . oryzae, *Chinese Chem. Lett.*, 2024, **35**, 109635.
23 M. Managa, E. Antunes and T. Nyokong, Conjugates of platinum nanoparticles with gallium tetra - (4-Carboxyphenyl) porphyrin and their use in photodynamic antimicrobial chemotherapy when in solution or embedded in electrospun fiber, *Polyhedron*, 2014, **76**, 94–101.
24 F. Matebese and N. Malomane, Porphyrin-Modified Polyethersulfone Ultrafiltration Membranes for Enhanced Bacterial Inactivation and Filtration Performance, *Membranes*, 2025, **15**, 239.
25 G. Heo, R. Manivannan, H. Kim, J. W. Ryu and Y.-A. Son, Visible Light Photo-Sensitized Metallo-Porphyrin/TiO_2 Photocatalyst and Its Related Self-Cleaning Effects in Poly Ethylene Terephthalate, *J. Nanosci. Nanotechnol.*, 2019, **19**, 8004–8012.
26 K. S. Ndlovu, K. Chokoe, T. Masebe, K. E. Sekhosana, M. J. Moloto and M. Managa, Photoinactivation of Escherichia coli and Staphylococcus aureus using

Porphyrin-CuInS$_2$/ZnS quantum dot conjugates immobilized on Mesoporous Silica, *Chem. Pap.*, 2024, **78**, 4991–5004.

27 L. C. Makola, M. Managa and T. Nyokong, Enhancement of photodynamic antimicrobialtherapy through the use of cationic indium porphyrin conjugated to Ag/CuFe$_2$O$_4$ nanoparticles, *Photodiagnosis Photodyn. Ther.*, 2020, **30**, 1–12.

28 Y. I. Openda, B. P. Ngoy, J. T. Muya and T. Nyokong, Synthesis, theoretical calculations and laser flash photolysis studies of selected amphiphilic porphyrin derivatives used as biofilm photodegradative materials, *New J. Chem.*, 2021, **45**, 17320–17331.

29 C. Comuzzi, A. Fiorot, A. Baggio, M. Maifreni, P. Strazzolini, M. Marino and S. Susmel, Imprinting Pentaphyrin on Conductive Electropolymerized Dipyrromethane Films: A New Strategy towards the Synthesis of Photokilling Materials, *Chempluschem*, 2020, **85**, 776–782.

30 S. Kavitha and V. Raghavan, Isolation and characterization of marine biofilm forming bacteria from a ship's hull, *Front. Biol.*, 2018, **13**, 208–214.

31 J. Chen, W. Wang, P. Hu, D. Wang, F. Lin, J. Xue, Z. Chen, Z. Iqbal and M. Huang, Dual antimicrobial actions on modified fabric leads to inactivation of drug-resistant bacteria, *Dye. Pigment.*, 2017, **140**, 236–243.

32 S. Bagheri, K. Shameli and S. B. Abd Hamid, Synthesis and characterization of anatase titanium dioxide nanoparticles using egg white solution *via* Sol–Gel method, *J. Chem.*, 2013, **2013**, 848205.

33 M. Al-Amin, S. Chandra Dey, T. U. Rashid, M. Ashaduzzaman and S. M. Shamsuddin, Solar Assisted Photocatalytic Degradation of Reactive Azo Dyes in Presence of Anatase Titanium Dioxide Energy extraction from the tectonic fault: A potential remedy from the devastating earthquake View project Biomaterials View project Solar Assisted Phot, *Int. J. Latest Res. Eng. Technol.*, 2016, **2**, 14–21.

34 C. E. Diaz-uribe, M. C. Daza, F. Martínez, E. A. Páez-mozo, C. L. B. Guedes and E. Di, Journal of Photochemistry and Photobiology A : Chemistry Visible light superoxide radical anion generation by tetra (4-carboxyphenyl) porphyrin/TiO$_2$: EPR characterization, *J. Photochem. Photobiol., A*, 2010, **215**, 172–178.

35 M. L. M. Budlayan, J. N. Patricio, J. P. Lagare-Oracion, S. D. Arco, A. C. Alguno, A. Basilio, F. S. Latayada and R. Y. Capangpangan, Improvised centrifugal spinning for the production of polystyrene microfibers from waste expanded polystyrene foam and its potential application for oil adsorption, *J. Eng. Appl. Sci.*, 2021, **68**, 1–11.

36 J. Fang, Y. Xuan and Q. Li, Preparation of polystyrene spheres in different particle sizes and assembly of the PS colloidal crystals, *Sci. China Technol. Sci.*, 2010, **53**, 3088–3093.

37 R. Naik, P. Joshi and R. K. Deshpande, Immobilization of metallporphyrins on polystyrene: Efficient catalysts for aerobic oxidation of alcohols, *J. Mol. Catal. A Chem.*, 2005, **238**, 46–50.

38 R. Naik, P. Joshi, S. Umbarkar and R. K. Deshpande, Polystyrene encapsulation of manganese porphyrins: Highly efficient catalysts for oxidation of olefins, *Catal. Commun.*, 2005, **6**, 125–129.

39 A. Wang, Q. Wu, C. Han, H. Yang and X. Xue, Significant influences of crystal structures on photocatalytic removal of NOx by TiO$_2$, *J. Photochem. Photobiol. A Chem.*, 2021, **407**, 113020.

40 A. B. D. Nandiyanto, R. Zaen and R. Oktiani, Correlation between crystallite size and photocatalytic performance of micrometer-sized monoclinic WO$_3$ particles, *Arab. J. Chem.*, 2020, **13**, 1283–1296.

41 F. Cummings and A. Tshaka, Opto-electronic properties of anodized TiO2 nanotube arrays investigated using electron energy loss spectroscopy, *Surf. Interfaces*, 2019, **17**, 100347.

42 L. C. Makola, M. Managa and T. Nyokong, Enhancement of photodynamic antimicrobialtherapy through the use of cationic indium porphyrin conjugated to Ag/CuFe$_2$O$_4$ nanoparticles, *Photodiagnosis Photodyn. Ther.*, 2020, **30**, 101736.

43 M. Managa, M. A. Idowu, E. Antunes and T. Nyokong, Photophysicochemical behavior and antimicrobial activity of dihydroxosilicon tris(diaquaplatinum) octacarboxyphthalocyanine, *Spectrochim. Acta, Part A Mol. Biomol. Spectrosc.*, 2014, **125**, 147–153.

44 D. V. Kladko, A. S. Falchevskaya, N. S. Serov and A. Y. Prilepskii, Nanomaterial shape influence on cell behavior, *Int. J. Mol. Sci.*, 2021, **22**, 5266.

45 N. B. Magaela, M. M. Ledwaba, N. Malomane, J. Mack, T. Nyokong and M. Managa, Photodynamic inactivation of Staphylococcus aureus and Escherichia coli with free-base and indium(III) 5,10,15,20-*tetrakis*(4-pyridyl) porphyrin adsorbed onto single-walled carbon nanotubes, *J. Porphyr. Phthalocyanines*, 2024, **28**, 260–271.

46 H. Wang, D. Zhou, Z. Wu, J. Wan, X. Zheng, L. Yu and D. L. Phillips, The visible light degradation activity and the photocatalytic mechanism of tetra(4-carboxyphenyl) porphyrin sensitized TiO$_2$, *Mater. Res. Bull.*, 2014, **57**, 311–319.

47 C. Song, Y. Li, J. Li, Y. Wei, H. YZ and W. Y, [Fluorescence spectra and quantum yield of TiO$_2$ nanocrystals synthesized by alcohothermal method], *Guang Pu Xue Yu Guang Pu Fen Xi*, 2008, **28**, 169–173.

48 T. Daimon and Y. Nosaka, Formation and behavior of singlet molecular oxygen in TiO$_2$ photocatalysis studied by detection of near-infrared phosphorescence, *J. Phys. Chem. C*, 2007, **111**, 4420–4424.

49 P. Y. Lee, J. Costumbrado, C. Y. Hsu and Y. H. Kim, Agarose gel electrophoresis for the separation of DNA fragments, *J. Vis. Exp.*, 2012, 1–5.

50 I. Aj Ibrahim, 16S rRNA gene sequencing for identification of some enterobacteriaceae species isolated from Trigris River, *Al-Mustansiriyah J. Sci.*, 2016, **27**, 13–16.

51 L. C. Makola, S. Mgidlana and T. Nyokong, Amphiphilic axially modified cationic indium-porphyrins linked to hydrophilic magnetic nanoparticles for photodynamic antimicrobial chemotherapy against gram-negative strain; Escherichia coli, *Dye. Pigment.*, 2021, **192**, 109262.

52 S. Yu, J. Shi, T. Sun, Z. Xie and L. Sun, Light-induced antimicrobial activities of porphyrin derivatives as photosensitizers, *APL Mater.*, 2024, **12**, 0213923.